

A study on continuous beam laser welding of dissimilar materials using Multi-Physics simulation

R Indhu, Sarathkumar Loganathan, L Vijayaraghavan, S Soundarapandian*

Indian Institute of Technology Madras, Chennai, TN, India

*Corresponding author: Department of Mechanical Engineering, IIT Madras-600036, sspandian@iitm.ac.in

Abstract:

Laser dissimilar welding finds its application mainly in the field of tailor-welded blanks (TWB). TWB combining steel to aluminium alloys are widely used in the automotive industry for achieving excellent lightweight structures thus it is enhancing the functional performance of the vehicle. A three-dimensional axisymmetric model of heat transfer and laminar fluid flow physics are developed to understand the complex physical phenomenon that governs the laser welding process. A Gaussian laser beam profile was used to study the effect of the power density of laser on the weld bead profile (weld depth and penetration depth). The model calculates the transient temperature profiles and the dimensions of the fusion zone. The effect of Marangoni convection on the weld width and weld depth penetration are also investigated in the model. The model calculations are compared with the experimental results of continuous laser welding. A small difference in the penetration depth (~65 μm) and weld width (~200 μm) were observed between the simulation and the experimental values. This difference might be because the change in absorptivity of laser when temperature increases was not considered in the model.

Keywords: Laser beam welding, Marangoni convection, absorption, steel, aluminum, weld bead profile.

1. Introduction

The growing demand for light weight automobiles to satisfy the environmental concerns are pushing the automotive industries towards weight reduction at the same time that has to maintain the structural integrity and crash worthiness of the vehicle. Hence the importance of lightweight materials in their design has been increasing in the automobile sectors [1]. As a result, the traditional materials such as cast iron and low carbon steels are being replaced with lightweight materials such as aluminium, magnesium and high strength steels. Advanced high strength steels (AHSS) and aluminium (Al) alloys are mostly used in automobile bodies due to their high

strength to weight ratio that enhances the performance of the vehicle.

Laser beam welding is a prominent technique than conventional welding methods to join steel and Al alloys, as it's a high energy density process and the high heating and cooling rates in laser welding inhibit the formation of brittle intermetallics. Dissimilar material laser welding finds its application mostly in Tailor Welded Blanks (TWB) where sheets of same or different thickness and material are welded together prior to forming process [2].

But joining of Al alloys to steel poses several problems such as brittle intermetallic formation, low wetting of steel to Al alloy due to their low miscibility during welding. This is because of the large difference in their thermo-physical properties such as melting temperatures (660° C for Al alloys and 1560° C for steels), dissimilar thermal expansion, heat capacity and thermal conductivity [3].

To understand the physical phenomena behind the welding process. It is necessary to build a model to predict the geometry of the weld bead (weld width and weld depth). A heat transfer and fluid flow model can help in predicting the final shape of the weld pool. The high intensity laser beam increases the temperature of the material beyond its melting point and sometimes beyond its boiling point [4]. Due to the large temperature gradients at the surface of the weld pool a phenomenon known as Marangoni convection occurs. The Marangoni convection controls the shape of the weld [5].

Numerous studies have been carried to simulate the laser welding process. Bachmann et al. [6] modeled the influence of a steady state magnetic field in keyhole welding of thick aluminium sheets. The flow pattern in the weld pool and the temperature distribution has significantly changed due to the application of steady magnetic field that produces a braking Lorentz force based on Hartmann Effect. The induced magnetic field has lowered the Marangoni convection. Courtois et al. [7] developed a two dimensional (2D) axial symmetric model to study the physical phenomena associated to the defects formation during welding. Level set method was used in the model and in this method the phase change from liquid to vapor was simulated. The interaction between the vapor

jet and the liquid surface was also analyzed. Guen et al. [8] developed a 3D thermal model to predict the deformed weld pool profile and a 2D hydrodynamic model to simulate the fluid flow around the keyhole.

In the current work, a three dimensional (3D) axial symmetry model for laser welding of dissimilar materials in conduction welding mode is developed. The goal is to predict the solid-liquid interface and the deformed weld pool shape under the influence of Marangoni convection and surface tension forces. To validate the model, experiments were carried out using a high power diode laser on dual phase steel and aluminium alloy in conduction mode. The model takes into account both heat transfer and fluid flow model. The temperature distribution of the weld pool and the weld pool geometry were compared with the experimental results.

2. Experimental setup

The experiments were carried out using a 6 kW high power diode laser in conduction welding mode. The laser with a wavelength of 980 nm, beam diameter of 1.5 mm and laser intensity distribution of top-hat profile was used. The materials used in this study were dual phase steel (DP 600) of 2.5 mm thick and Al alloy (AA 6061) of 3 mm thickness with a dimension of 120 mm × 40 mm. The laser head was tilted to an angle of 5° along the weld axis to avoid backscattering of the laser beam that could damage the laser optics. The stand-off distance between the optical lens and the workpiece was maintained to 85 mm. Argon (Ar) shielding gas was used with a pressure of 0.5 bar to avoid the oxidation of the molten weld pool. Fig 1 shows the experimental set up of laser used for welding of DP steel and Al 6061 coupons.

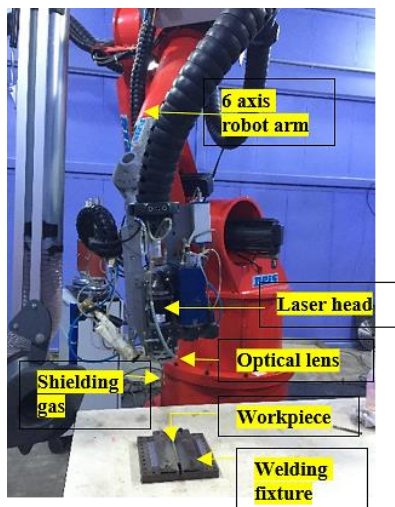


Fig. 1 Experimental set up of laser welding.

The laser parameters are varied according to energy density of the laser beam which is calculated using Eq. 1. The laser parameters used in the experiments and modeling as given in Table. 1.

$$\begin{aligned} \text{Laser energy density (LED)} &= \frac{\text{Laser power}}{\text{Unit area}} \times \frac{\text{Laser beam diameter}}{\text{Scanning speed}} \\ \text{LED} &= \frac{4P}{\pi D^2} \times \frac{D}{V} \end{aligned} \quad (1)$$

Where, P is the laser power (kW), D is the diameter of the laser beam (mm) and V is the scanning speed of laser beam (mm/s).

Table. 1 Laser parameters used in experimentation and modeling.

S. No	Laser power (kW)	Scanning speed (mm/s)	LED (J/mm ²)
1	3.5	8	371
2	3.5	10	297

3. Mathematical Formulations

A 3D computational model was developed to understand the dependence of the flow pattern and surface tension gradient on the resulting melt pool shape on the weld. The computational model that has incorporated the Multiphysics effects (heat transfer and laminar fluid flow) for predicting the temperature histories, cooling rates and the fluid flow inside the molten pool.

For heat transfer and fluid flow modeling, the equations of conservation of energy, (Eq.2) momentum (Eq. 3) and mass (Eq. 4) are solved. The following assumptions are made in the model.

1. Liquid metal is considered to be incompressible Newtonian under flow.
2. Gaussian heat source.
3. Boussinesq approximation valid.

$$\begin{aligned} \rho C_p \frac{\partial T}{\partial t} + \rho C_p u \cdot \nabla &= \frac{\partial}{\partial x} \left(k \frac{\partial T}{\partial x} \right) + \frac{\partial}{\partial y} \left(k \frac{\partial T}{\partial y} \right) \\ &+ \frac{\partial}{\partial z} \left(k \frac{\partial T}{\partial z} \right) \end{aligned} \quad (2)$$

Where, ρ is the density (Kg/m³), C_p is the specific heat of the material (J/Kg.K), u is the velocity of the molten metal and T is the absolute temperature. The initial

condition is given by Eq. 3, where the initial temperature T_0 is maintained at 293 K.

$$T(x, y, z, 0) = T_0 \quad (3)$$

The convective cooling and surface to ambient radiation boundary conditions was assigned to the whole geometry except the bottom surface as shown in Fig. 2 and the thermal insulation was assigned to the bottom of the geometry. The boundary conditions and the heat flux is expressed in Eq. 4.

$$-k\nabla T = -Q + h[T - T_0] + \varepsilon\sigma[T^4 - T_0^4] \quad (4)$$

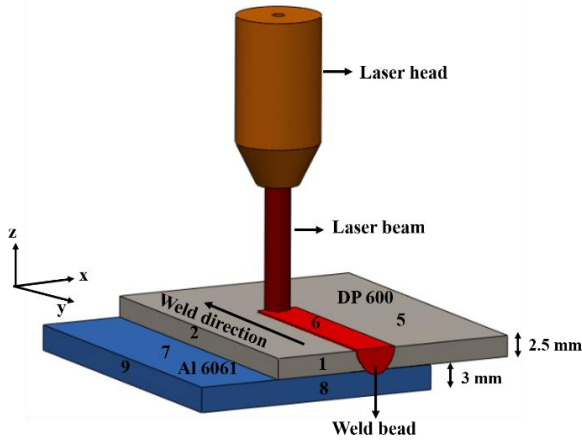


Fig. 2 Schematic of laser welding process.

The model uses a Gaussian heat source distribution and the power density, which is expressed in Eq. 5 to boundary 6 in Fig. 2. In Eq. 2 the laser intensity is not in the source term and therefore defined as a separate boundary condition as heat flux (Eq. 5) in the heat transfer module.

$$Q = A_c \cdot \frac{P}{\pi D^2} \cdot \exp\left[-\left(\frac{(x-x_0)^2}{2\phi^2}\right)\right] \cdot \exp\left[-\left(\frac{(y-y_0)^2}{2\phi^2}\right)\right] \quad (5)$$

The heat transfer model was incorporated with the fluid flow Multiphysics to determine the deformation of the molten weld pool under various boundary conditions such as Marangoni convection, gravitational forces and surface tension forces to predict the weld bead morphology. The equations of mass (Eq. 6) and momentum (Navier-Stokes, Eq. 7) conservation were used to govern the fluid flow in the weld.

$$\nabla \cdot u = 0 \quad (6)$$

$$\rho \frac{\partial u}{\partial T} + \rho(u \cdot \nabla)u = \nabla \cdot [-pl + \mu(\nabla u + (\nabla u)^T)] - \rho(1 - \beta(T - T_m))g + F \quad (7)$$

Where, F is the volume force (N), g is the acceleration due to gravity, α is the coefficient of thermal expansion (1/K) and T_m is the melting temperature.

$$F = \rho g \alpha (T - T_m) \quad (8)$$

Marangoni convection is a fluid flow due to the surface tension in the molten weld pool. The Marangoni convection is assigned to the boundary 6 on the top surface

$$-\mu \frac{\partial u}{\partial x} = \frac{\partial T}{\partial y} \cdot \frac{\partial \gamma}{\partial T} \quad (9)$$

Where, μ is the dynamic viscosity (Pa-s) and γ is the temperature derivative of surface tension. The material properties. Temperature dependent specific heat and thermal conductivity and the laser machining parameters are summarized in Table. 2, Table. 3 and Table. 4.

Table. 2 Material properties of DP 600 steel and Al 6061 alloy

Property	Nomenclature	Value (units)	
		DP 600	Al 6061
Density	ρ	7594[kg/m ³]	2830[kg/m ³]
Temperature derivative of surface tension	γ	-0.43e-3 [N/(m.K)]	-3.5e-4 [N/(m.K)]
Thermal expansion coefficient	α	1.96e-5[1/K]	2.7e-5[1/K]
Dynamic viscosity	μ	8[(m*Pa)/s]	1.15 [(m*Pa)/s]
Convection coefficient	Ψ	73.5 [W/m ² *K]	2975 [W/m ² *K]
Emissivity	E	0.25	0.1

Table. 3 Temperature dependent thermal properties of DP 600 steel and Al 6061 alloy

Temperature dependent specific heat and conductivity of DP 600							
DP 600 [9]				Al 6061 [10]			
Specific heat C_p [J/(kg*K)]		Thermal conductivity k[W/(m*K)]		Specific heat C_p [J/(kg*K)]		Thermal conductivity k[W/(m*K)]	
T°	Value	T°	Value	T°	Value	T°	Value
0	520	0	34.6	20	809	20	114.3
200	550	25	34.8	100	860	100	122.3
400	600	200	35	200	897	200	130.8
600	750	254	35	300	922	300	145.1
740	1160	1100	21.4	400	872	400	124.5
800	690	1200	25.5	500	985	500	122.7
1100	520	1300	60				
1200	610	1400	70				
3000	620	3000	70				

A free tetrahedral mesh with a maximum element size of 15 μm and a minimum of 0.6 μm were generated for the boundary 6 along the melting zone. A very fine mesh was

generated for the rest of the domains where the influence of the heat source is minimum. The computational model was solved for small time steps (0.001s for $t < 4s$) to study the minute temperature variation during welding. Point domain probes were placed as cross-sectionally from the top to bottom surface to track the variation of temperature in each time steps.

Table. 4 Laser machining parameters

Parameter	Nomenclature	Value (units)
Laser power	P	kW
Scanning speed	V	mm/s
Laser beam diameter	d	1.5 [mm]
Absorptivity	A_c	0.35
Heat transfer coefficient	h	15 (W/m ² *K)
Standard deviation of laser beam	ϕ	0.3[mm]
Ambient temperature	T_0	293 [K]
Stefan Boltzmann constant	σ	5.67×10^{-8} (W/m ² K ⁴)

4. Results and Discussion

A 3D model was developed (Fig. 3) to study the effect of a moving laser beam on the final shape of the weld. The rise and drop of the temperature at higher laser intensities, convection and radiation losses and the fluid flow in the molten pool by Marangoni convection and surface tension forces greatly influence the weld bead morphology. A Gaussian laser beam generates high intensity at the center compared to the edges, which results in non-uniform weld shape with a maximum penetration depth at the center of the beam.

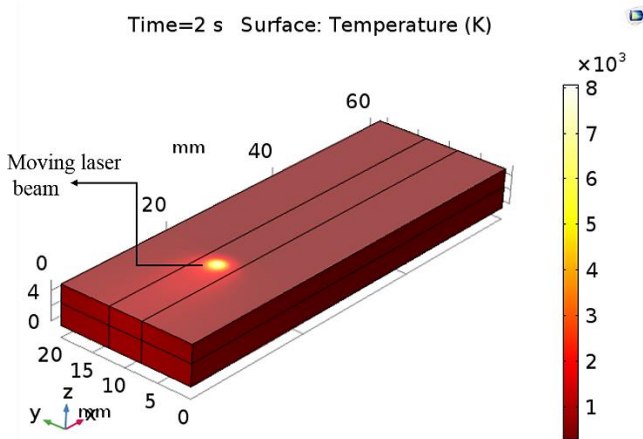


Fig. 3 Three dimensional view of laser beam welding process.

Laser energy density (LED) plays a vital role in the formation of the weld bead. It was observed from the model that the peak temperature increases with increase in

LED. Owing to the increase in temperature, the amount of heat conducted into the material increases resulting in higher penetration depth. At a LED of 371 J/mm² the model generated a weld width of 6400 μ m and a depth of 789 μ m (Fig. 4). At a lower LED of 297 J/mm² the weld width and penetration depth reduced to 5410 μ m and 393 μ m as shown in Fig. 5.

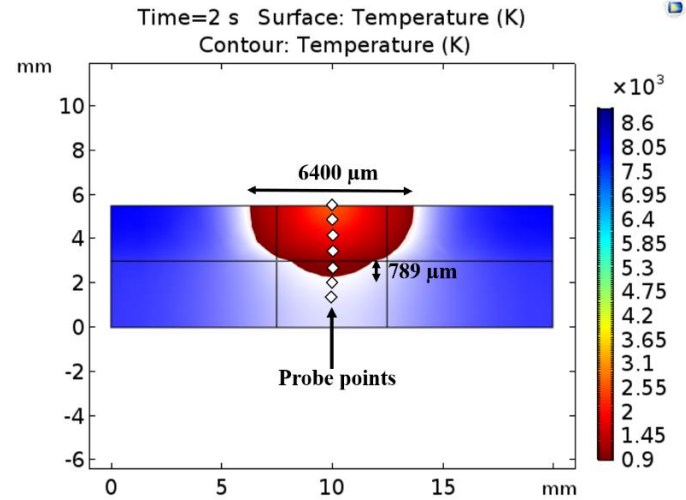


Fig. 4 Temperature distribution along YZ plane and shape of the weld bead at a LED of 371 J/mm².

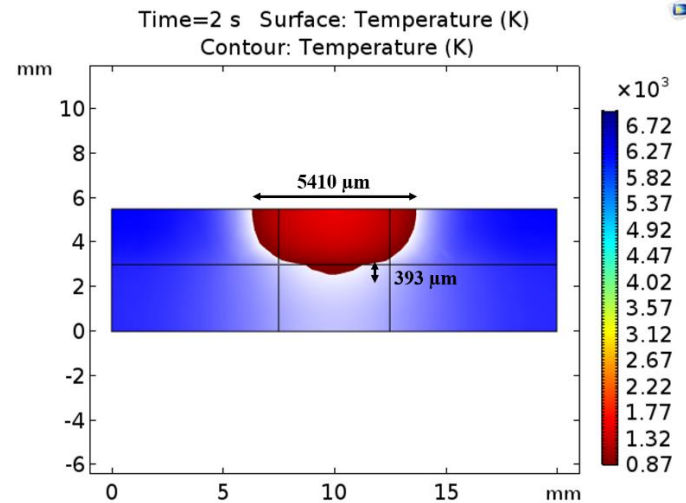


Fig. 5 Temperature distribution along YZ plane and shape of the weld bead at a LED of 297 J/mm².

The temperature profile was extracted from boundary 6 using the domain point probes (Fig. 4) that were placed along the cross-section of the weld in the YZ plane. The temperature profile depicting the heating time and the cooling time for both the cases at a LED (371 J/mm² and 297 J/mm²) are shown in Fig. 6 and 7. At higher LED (371 J/mm²) i.e., at lower scanning speed (8 mm/s), the laser remains in contact with the material for a longer duration

of time resulting in increased heating time of 0.4 s and higher peak temperature of ~ 8200 K. As the LED decreases (297 J/mm^2), the heating time reduced to 0.25 s with much lesser peak temperature of ~ 7800 K. Another important phenomena that governs the weld width and the depth is the Marangoni convection forces. Marangoni effect is the mass transfer that occurs due to the gradient in the surface tension in the molten weld pool.

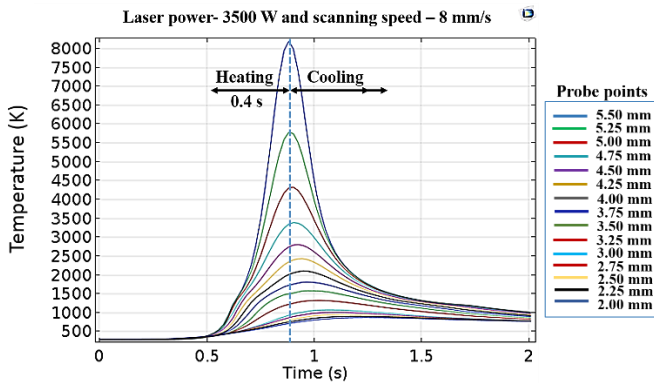


Fig.6 Plot of probe point temperature along the YZ plane at a LED of 371 J/mm^2 .

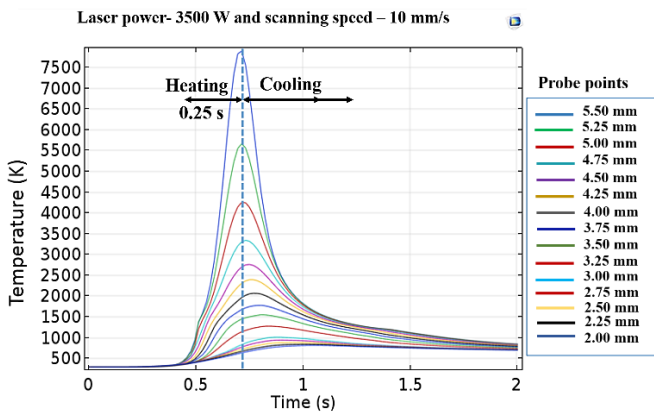


Fig. 7 Plot of probe point temperature along the YZ at a LED of 297 J/mm^2 .

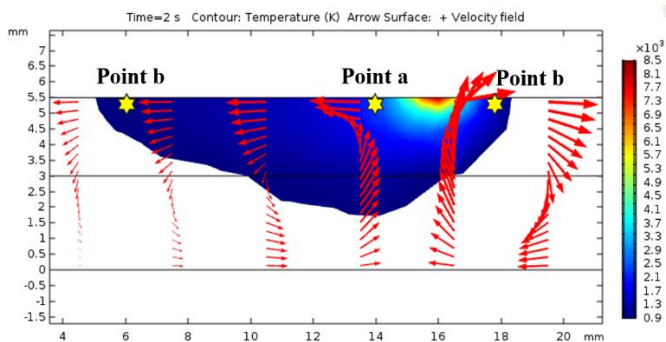


Fig. 8 Effect of Marangoni convection in the weld pool due to the difference in temperature gradient at a LED of 371 J/mm^2 .

The surface tension of the molten metal increases with increase in temperature. The warmer liquid at point ‘a’ has lower surface tension and is pulled towards point ‘b’ (Fig. 8). The surface tension gradient along the molten pool causes an outward shear stress [11]. This results in the movement of the molten metal from the center of the weld to the edges of the pool and return below the pool surface as shown in Fig. 8. At higher LED the Marangoni convection increases resulting in larger weld width. The influence of surface tension and gravitational forces were minimum when compared to the Marangoni convection forces acting in the weld.

Fig. 9 and Fig. 10 shows the experimental results of the welding process at a LED of 371 J/mm^2 and 297 J/mm^2 .

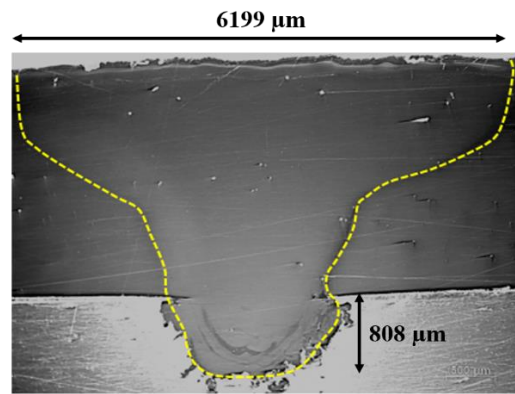


Fig. 9 Optical micrograph of the weld bead at a LED of 371 J/mm^2 .

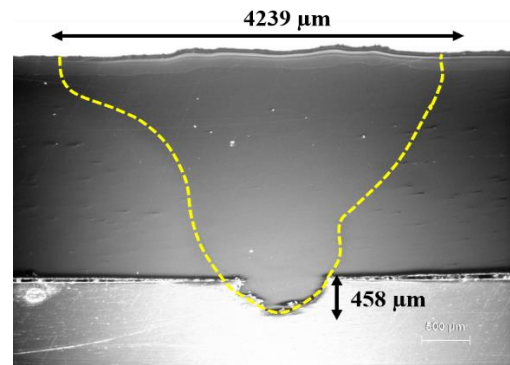


Fig. 10 Optical micrograph of the weld bead at a LED of 297 J/mm^2 .

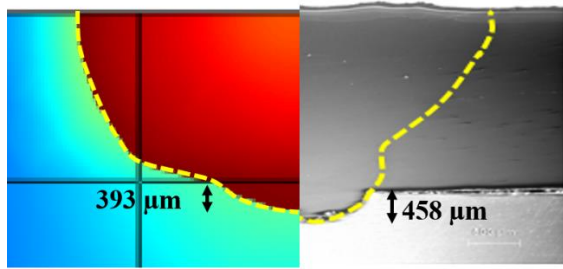


Fig. 11 Comparison of computational and experimental weld bead profile at a laser power of a LED of 297 J/mm².

A comparison between the experiment and the simulation result at a LED of 297 J/mm² is shown in Fig. 11. The slight difference in the shape could be due to the fact that the beam profile used in the experiments were slightly modified, which was not considered during modeling. There was a minimal difference in penetration depth (~ 65 μm) and weld width (~ 200 μm) between the model and simulation. The reason could be that as the temperature of the material increases there is a change in the absorptivity of the laser which was not taken into account in the model.

5. Conclusions

The current work presents the preliminary results concerning laser welding of dissimilar materials. The influence of laser parameters such as laser power, scanning speed and laser beam diameter on the shape of the weld bead (weld width and weld depth) was studied numerically and experimentally. The effect of Marangoni convection, gravity forces and surface tension forces on the molten weld were also analyzed.

It was shown that the solid-liquid interface of the weld was mainly governed by the Marangoni forces. The effect of gravity and the surface tension were found to be less significant than the Marangoni convection. The Marangoni convection tends to increase the weld width at lower scanning speed of 8 mm/s due to larger temperature gradient in the molten weld pool. The computational results showed a good qualitative agreement with the corresponding experimental values. The slight difference in the penetration depth and weld width. This could be because the model did not take into account the change in laser absorptivity values with increase in temperature.

References

- [1] E. Schubert, M. Klassen, I. Zerner, C. Walz, G. Sepold, Light-weight structures produced by laser beam joining for future applications in automobile and aerospace industry, *J. Mater. Process. Technol.* 115 (2001) 2–8. doi:10.1016/S0924-0136(01)00756-7.
- [2] D. Anand, D.L. Chen, S.D. Bhole, P. Andreychuk, G. Boudreau, Fatigue behavior of tailor (laser)-welded blanks for automotive applications, *Mater. Sci. Eng. A.* 420 (2006) 199–207. doi:10.1016/j.msea.2006.01.075.
- [3] G. Pardal, S. Meco, S. Ganguly, S. Williams, Dissimilar metal laser spot joining of steel to aluminium in conduction mode, *Int J AdvManuf Technol.* (2014) 365–373. doi:10.1007/s00170-014-5802-y.
- [4] S. Sharma, Y. Pachaury, S.N. Akhtar, M. Jabalpur, A study on hydrodynamics of melt expulsion in pulsed Nd : YAG laser drilling of titanium, *Proc. 2015 COMSOL Conf.* (2015). doi:https://www.comsol.com/paper/a-study-on-hydrodynamics-of-melt-expulsion-in-pulsed-nd-yag-laser-drilling-of-ti-30041.
- [5] C. Limmaneevichitr, S. Kou, Visualization of Marangoni convection in simulated weld pools containing a surface-active agent, *Weld. J.* 79 (2000) 324s–330s.
- [6] M. Bachmann, V. Avilov, A. Gumenyuk, M. Rethmeier, Multiphysics Process Simulation of the Electromagnetic-Supported Laser Beam Welding, *Mater. Res.* (2011) 1–3.
- [7] M. et. al Courtois, Keyhole Formation During Spot Laser Welding: Heat and Fluid Flow Modeling in a 2D Axisymmetric Configuration, *COMSOL Conf.* (2012) 1–6. https://www.comsol.com/paper/download/151897/courtois_paper.pdf.
- [8] E. Le Guen, R. Fabbro, F. Coste, Modeling 2D and 3D of Hybrid Laser Nd: Yag-MIG Welding Processes, Excerpt from Proceedings COMSOL Conf. 2008 Hann. (2008) 94114. http://www.comsol.com/papers/5214/download/LeGuen.pdf.
- [9] T.J. McInerney, R.B. Madigan, Trends in Welding Research-Proceedings of the 7th International Conference, ASM International Materials, 2005.
- [10] Y. Zhang, Y. Yi, S. Huang, H. He, Influence of Temperature-Dependent Properties of Aluminum Alloy on Evolution of Plastic Strain and Residual Stress during Quenching Process, *Metals (Basel)*. 7 (2017) 228. doi:10.3390/met7060228.
- [11] Sindo Kou, *Welding Metallurgy-Second Edition*, 2003. doi:10.1016/j.theochem.2007.07.017.